Wrinkled Nanoporous Gold Films with Ultrahigh Surface-Enhanced Raman Scattering Enhancement

Ling Zhang,[†] Xingyou Lang,[†] Akihiko Hirata,[†] and Mingwei Chen[†,‡,*]

[†]WPI Advanced Institute for Materials Research, Tohoku University, Sendai 980-8577, Japan, and [‡]State Key Laboratory of Metal Matrix Composites, School of Materials Science and Engineering, Shanghai Jiao Tong University, Shanghai 200030, PR China

ABSTRACT Amplified by plasmonic nanostructured metals, Raman intensity of organic molecules and biomolecules can be dramatically improved, particularly at "hot spots" where intense electromagnetic fields are produced in the vicinity of narrow nanogaps between metallic nanostructures. Therefore, developing new substrates with a high density of "hot spots" has been the recent topic of intense study. Here we report wrinkled nanoporous gold films that contain abundant Raman-active nanogaps produced by deformation and fracture of nanowire-like gold ligaments. This novel nanostructure yields ultrahigh surface enhanced Raman scattering for molecule detection.

KEYWORDS: wrinkle · nanoporous gold (NPG) · surface-enhanced Raman scattering (SERS) · nanogaps

Plasmonic-based Raman spectroscopy is one of the most promising techniques to probe and identify molecules for molecular diagnostics.[1−4] In general, normal Raman scattering of organic molecules and biomolecules is extremely weak due to the small cross section, typically in the range of 10^{-30}–10^{-25} cm^2. Amplified by surface plasmonics of nanostructured metals, the intensity of the surface-enhanced Raman scattering (SERS) can be dramatically improved by a factor of up to 10 orders of magnitude,[5−7] particularly, at "hot spots" where huge electromagnetic fields are produced in the vicinity of narrow nanogaps between sharp corners and edges of nanostructured noble metals.[8−11] Accordingly, it becomes possible to detect and distinguish the spectroscopic signature of a single molecule by SERS,[2,12−14] and developing novel nanostructured metals with a high density of "hot spots" has been the recent topic of intense discussion.[9,11,15] It has long been known that a quasi-periodic wrinkle of thin metal films can be produced by thermal contraction of an underlying prestrained polymer substrate (PS).[16,17] Wrinkling can turn the two-dimensional flat films to three dimensions (3D) along with rich nanostructures as effective plasmonic substrates.[18−20] In this study, we report wrinkled nanoporous gold (NPG) films that contain a high density of SERS-active nanogaps and sharp nanotips. This novel nanostructure with a local enhancement factor of ~10^9 shows over 100 times improvement in the SERS enhancement compared to flat NPG films.

RESULTS AND DISCUSSION

Wrinkled nanoporous gold films were prepared by thermal contraction of the NPG/PS composites (see the Experimental Methods). As shown in Figure 1, the annealing process leads to more than 50% shrinkage of the PS substrates and the formation of wrinkled nanoporous films. The microstructure of three as-prepared NPG films used in this study is illustrated in Figure 2a−c. Noticeable size difference in both nanopores and gold ligaments can be observed, and shorter dealloying time results in smaller nanopore sizes.[21−24] As revealed by electron tomography, the dealloyed NPG possesses bicontinuous nanoporosity, and free etching leads to the nearly identical nanopores and ligaments in size, geometry, and topology.[25] The low-magnification SEM micrograph (Figure 2d) shows as an example that the as-prepared NPG film is flat on a micrometer scale. The dark and bright contrast with a domain size of about several micrometers may be associated with the original grains of the precursor $Au_{35}Ag_{65}$ alloy. After annealing at 160 °C for 6 min, the shrinking of the PS substrate leads to the formation of a wrinkled NPG film (Figure 2e). The distribution of the wrinkles is uniform across the entire film with a biaxial periodicity. Along the primary wrinkle direction, the wavelength is of *ca.* 3−5 μm while the secondary direction has a wavelength of *ca.* 20−30 μm. The biaxial wrinkling gives rise to rose-petal-shape 3D nanostructure as shown in the zoom-in SEM images (Figure 2f−h).

* Address correspondence to mwchen@wpi-aimr.tohoku.ac.jp.

Received for review December 1, 2010 and accepted May 31, 2011.

Published online May 31, 2011
10.1021/nn201443p

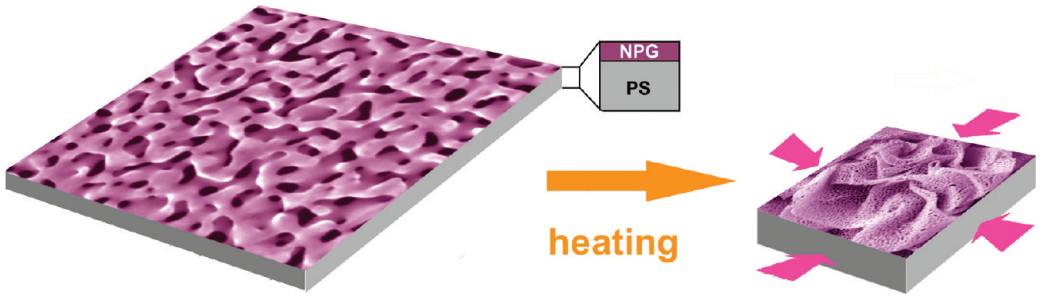

Figure 1. Schematic diagram of the wrinkled nanoporous gold films by thermal contraction of a prestrained polymer sheet.

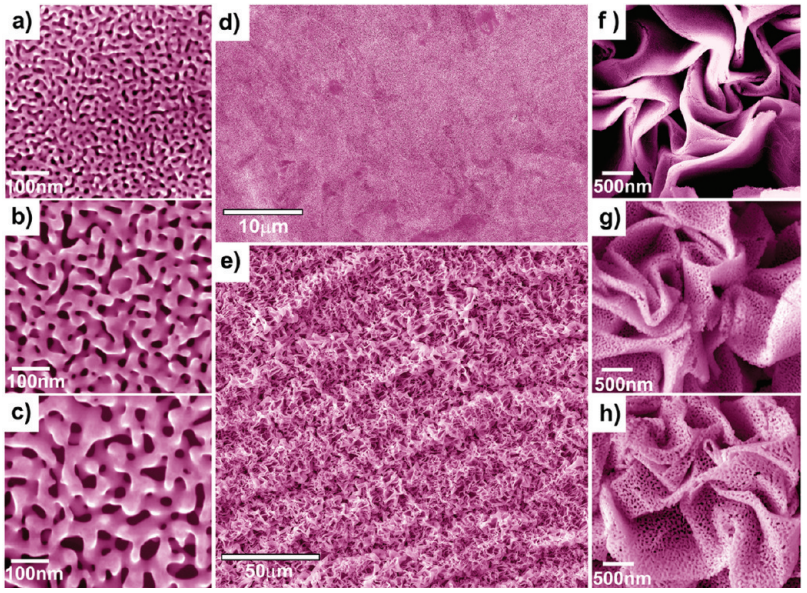

Figure 2. Microstructure of as-prepared NPG and wrinkled NPG films. (a–c) SEM micrographs of the as-prepared NPG films with different nanopore sizes of ~12 (a), 26 (b), and 38 nm (c); (d) SEM micrograph of an as-prepared NPG film with a nanopore size of ~38 nm showing the flat feature; (e) microstructure of a wrinkled NPG film with a pore size of ~38 nm; and (f–h) zoom-in SEM micrographs showing the local microstructures of the wrinkled NPG films with nanopore sizes of ~12 (f), 26 (g), and 38 nm (h), respectively.

It is worth noting that the wrinkling treatment does not cause any obvious change in nanoporosity of NPG except slight coarsening of nanopores and gold ligaments. The length scale of the wrinkles appears to be solely controlled by the contraction ratios but independent of nanopore sizes, since the wrinkle structures of the three samples are very analogous to each other. Owing to the large deformation of the NPG films caused by wrinkling, cracks can be frequently observed along the ridges of wrinkles from the 12 and 26 nm NPG samples (Figure 3a,b). In general, the fracture of the wrinkled 12 nm NPG (w-NPG12) films takes place in a brittle manner with a sharp-cut crack edge, whereas detectable plastic deformation of ligaments can be observed from the cracked ridges of the 26 nm NPG (w-NPG26) samples. In contrast, cracks are rarely seen from the wrinkled 38 nm NPG (w-NPG38) films in which the ligaments at the top of ridges appear to be plastically deformed in a ductile manner (Figure 3c). This observation is consistent with the previous report about the size dependent brittle-to-ductile transition of NPG.[26] For the w-NPG26 sample, the ridge cracks have a width ranging from smaller than one nanometer to tens of nanometers, which forms various nanogaps edged with fractured gold ligaments (Figure 3d,e). STEM characterization reveals that the broken ligaments have apexes less than 5 nm in diameter, which is much smaller than the original ligaments of the as-prepared sample. Deformation defects, such as deformation twins and stacking faults, can be frequently observed in the ligament, indicating that the formation of the sharp tips is associated with the localized plastic deformation of gold ligament during breaking.

To reveal the distribution of surface plasmonics of the heterogeneous nanostructure, the fluorescence images of CV molecules on the w-NPG26 film were studied by an OLYMPUS fluorescence microscope (for details, please see the Experimental Methods). With the exposure time of 2 s, the wrinkle structure with bright ridges and dark valleys can be well recognized (Figure 4a). Since fluorescence contrast directly relates to the intensity of local

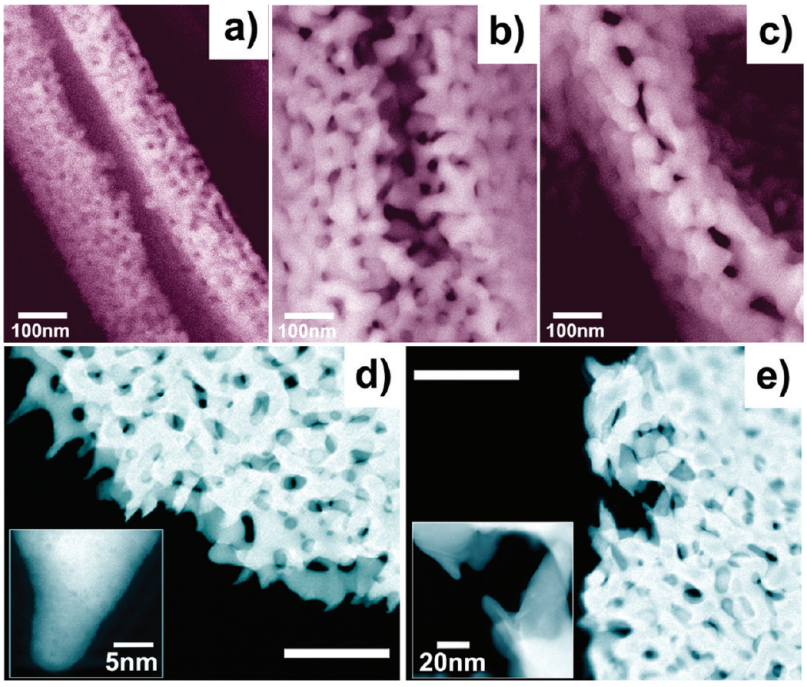

Figure 3. SEM and STEM micrographs of wrinkled NPG. (a−c) The ridges of the wrinkled NPG with the nanopore sizes of ~12 (a), 26 (b) and 38 (c). (d,e) STEM images of the fractured ridges of the wrinkled NPG with a nanopore size of 26 nm. The inserts of paneld d and e show individual sharp nanotips. The scale bars shown in panels d and e are 200 nm.

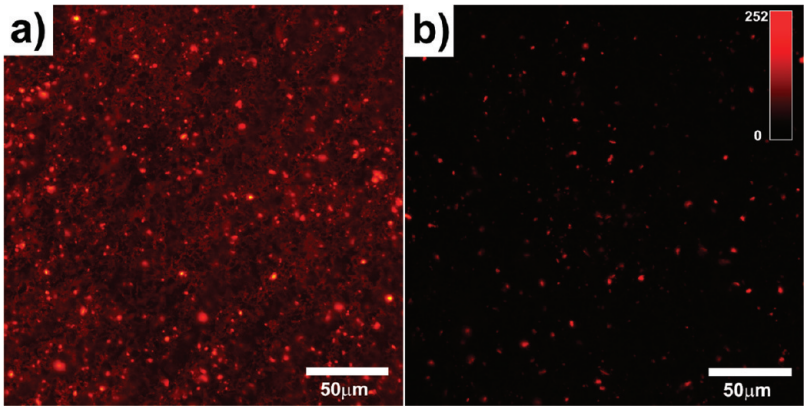

Figure 4. Fluorescence images of CV molecules on a HSA-functionalized 26 nm wrinkled NPG film with a green excitation. (a) Fluorescence image with the exposure time of 2 s and (b) fluorescence image with short exposure time of 100 ms. The CCD camera is saturated by a large number of bright spots even though the exposure time is only 100 ms.

electromagnetic fields, the bright ridges of the wrinkles apparently bring in more intense surface plasmon resonance. With short exposure time (100 ms), a high density of bright spots that always saturates the CCD camera can still be observed approximately along the wrinkle edges, which may correspond to the electromagnetic "hot spots" at the nanogaps of the cracked wrinkle ridges (Figure 4b).

The wrinkled NPG substrates were immersed in the 10^{-8} M CV solution for about 2 h, washed with methanol, and then dried in the air for SERS measurements, by which a submonolayer of CV molecules can be deposited on the substrates with a coverage ratio of $\sim 2.5 \times 10^3$ molecules per μm^2.[27] The laser beam size for the Raman measurements is set as large as $\sim 5\ \mu m$ in diameter to acquire averaged SERS spectra. As shown in Figure 5a, the wrinkling leads to obvious improvement in the SERS enhancements of the three samples in comparison with the flat NPG films. The enhancements show strong nanopore size dependence, and the wrinkled NPG with the nanopore size of ~26 nm exhibits the highest enhancement, that is, ~60-fold higher than that of the as-prepared NPG. Correspondingly, the Raman intensity of the wrinkled NPG films with nanopore sizes of ~12 nm and ~38 nm are about 20-fold and 50-fold stronger than those of their flat counterparts, respectively. Although the SERS enhancement of as-prepared NPG increases with

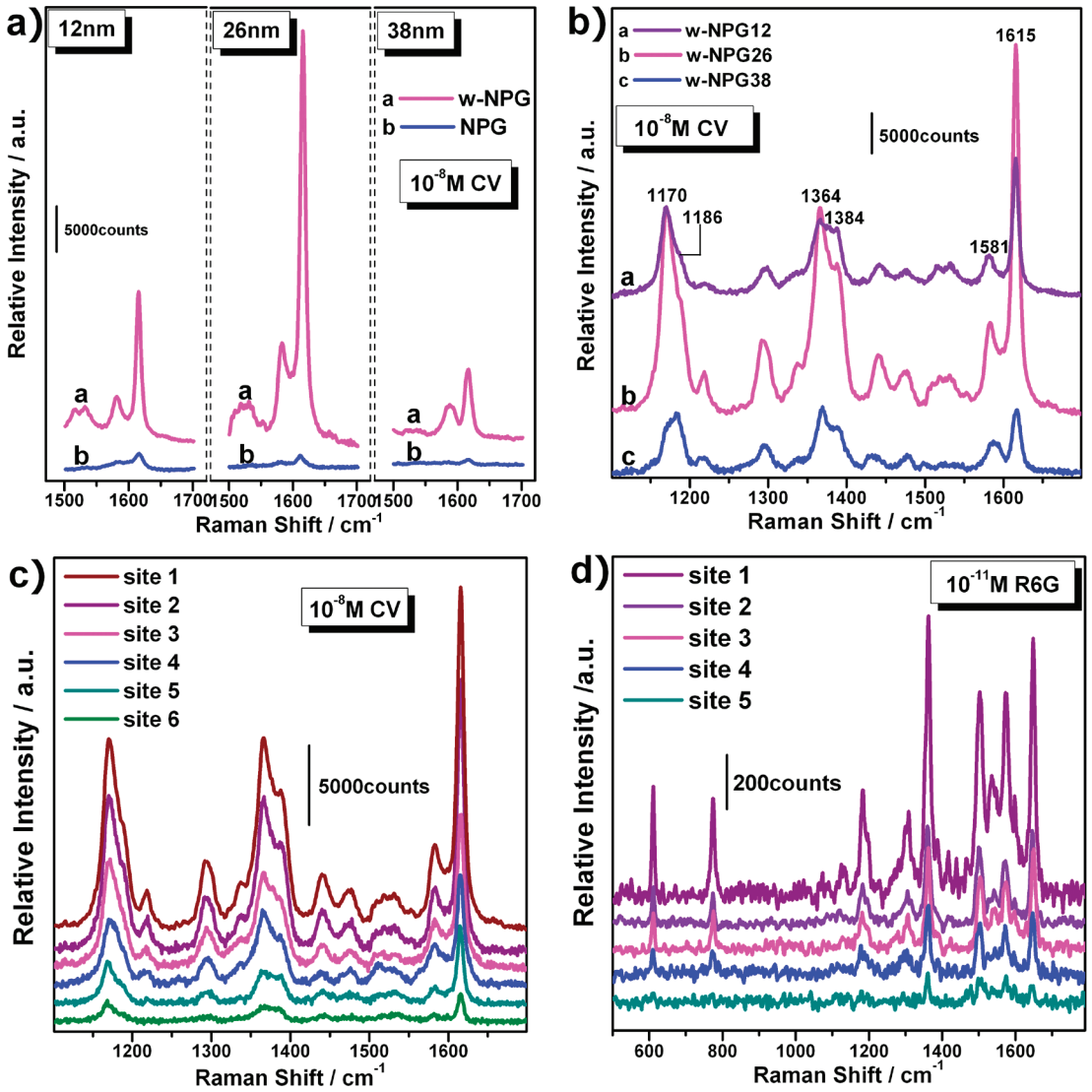

Figure 5. SERS spectra of CV and R6G molecules on wrinkled NPG films. (a) Comparison of SERS intensity between wrinkled and as-prepared NPGs with different nanopore sizes. (b) SERS spectra from wrinkled NPG with different nanopore sizes of 12 (w-NPG12), 26 (w-NPG26), and 38 nm (w-NPG38). (c) Variation of SERS spectra of CV on w-NPG26 at different sites along a wrinkle ridge. (d) Variation of SERRS spectra of R6G on w-NPG26 at different sites along a wrinkle ridge. The excitation wavelength is 632.8 nm for CV and 514.5 nm for R6G.

nanopore sizes decreasing[21] and the sample with the smallest pore size of ~12 nm possesses the highest SERS enhancement among the three as-prepared samples, the strongest SERS enhancement of the wrinkled samples is observed from the one with a pore size of ~26 nm (Figure 5b), suggesting the microstructure changes caused by wrinkling play an dominant role in the improved SERS effect. In addition to the nanopore size effect, the contraction ratios of the wrinkled NPG films also affect the SERS property and high contraction ratios provide better SERS enhancements. (see Figure S1 in the Supporting Information). With a small laser beam size of ~1 μm in diameter, we investigated the SERS inhomogeneity of the wrinkled NPG films by acquiring the Raman signals from different sites. Consistent with the fluorescence image, the bright ridges of the wrinkles offer much stronger SERS signals than the dark valleys. Moreover, scanning along a wrinkle ridge, one can find that the Raman intensity also changes dramatically from site to site. The enhancements from the sites that may correspond to "hot spots" are more than ten times stronger than those of the weakest ones at the ridges (Figure 5c,d).

The enhancement factor (EF) of the wrinkled NPG film with the nanopore size of 26 nm is measured by dilute solutions of 10^{-11} M R6G with 514.5 nm laser excitation. A 2 μL droplet of the 10^{-11} M R6G methanol solution is dropped on the wrinkled NPG substrate. The solution diffuses on the surface to form a blot with a diameter of 0.8 cm. To avoid the coffee stain effect, the measurements are carried out in the center of the droplet with a laser beam of ~2 μm in diameter. For reference, a 2 μL droplet of a 0.01 M R6G methanol solution is dropped on a single-crystal gold flat surface

with a diameter of 0.8 cm for the resonance Raman scattering (RRS) measurements. The EF is calculated by comparing the intensity of the single molecule from the surface-enhanced resonance Raman scattering (SERRS) signal with that from the RRS signal by the formula[28−30]

$$EF = (I_{SERRS}/N_{SERRS})/(I_{RRS}/N_{RRS}) \quad (1)$$

where N_{RRS} is the number of probe molecules contributing to the bulk Raman signal, N_{SERRS} is the number of probe molecules contributing to the SERRS signal, and I_{SERRS} and I_{RRS} are the intensities of the selected scattering bands in the SERRS and resonance Raman spectra, respectively (Figure 6). The probed molecules are assumed to distribute on the substrates uniformly. Since the specimens for RRS and SERRS detection are prepared in the same way, the number of the detected molecule can be estimated by

$$N = (N_A M V_{solution}/S_{sub})S_{laser} \quad (2)$$

where N_A is Avogadro constant, M is the molar concentration of the solution, $V_{solution}$ is the volume of the droplet, S_{sub} is the size of the substrate, and S_{laser} is the size of the laser spot. The relevant data required by eq 1 and eq 2 are listed in Table 1. On the basis of the SERRS and RRS measurements (Figure 6), the average EF of the winkled NPG is estimated to be $\sim 0.7 \times 10^8$, much higher than that of the flat single-crystal gold foil and original NPG ($\sim 10^6$). Since the magnitude of the intensity at the best enhanced sites is more than ten times larger than that at the weak enhanced sites, as shown in Figure 5c,d, the local EF at the "hot spots" is approximately larger than 10^9, approaching the requirement for single molecule detection.[5]

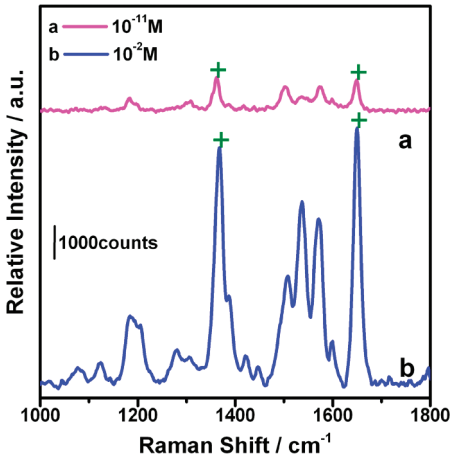

Figure 6. SERRS spectrum of R6G adsorbed on w-NPG26 film and RRS spectrum of R6G located on single crystal gold foil (excitation, 514.5 nm).

To understand the enhancement mechanisms of the wrinkled NPG films, three pairs of the characteristic Raman bands of the CV molecules (Table 2) are investigated, each pair consists of one polarized band (p) and one depolarized band (dp).[31−33] The p vibrations are totally symmetric whereas the dp vibrations are nontotally symmetric. In general, if the SERS enhancement originates from the chemical effect, the strong chemical interaction between probed molecules and substrates leads to the Raman band shift of ~ 20 cm^{-1}.[32] It can be seen that the SERS band shift observed in this study is very small when compared with that in the FT-Raman spectra reported in the literature[32] (Table 2), suggesting that the chemical interaction between CV molecules and the wrinkled NPG substrates is very weak. According to Herzberg−Teller-surface selection rules, nontotally symmetric modes are mostly enhanced by proximity of CV molecules to the metal surfaces. Thus, if the chemical enhancement from charge transfer plays a key role in the enhancement effect, the dp modes should show the strongest enhancements in the SERS spectra.[32] However, for the w-NPG, the totally symmetric p modes at 1170 and 1617 cm^{-1} are the most intense modes, (Figure S2 in the Supporting Information), further demonstrating the less chemical

TABLE 2. Assignments of the Characteristic Vibrational Modes of Crystal Violet[a]

	SERS				
FT-Raman[c]	12 nm	26 nm	38 nm	assignment[b]	polarity[c]
1170(m)	1170(s)	1171(s)	1177(m)	ring C—H bending	p
1185(m)	1186(m)	1187(m)	1188(s)	ring C—H bending	dp
1357(s)	1364(s)	1367(s)	1369(s)	N-phenyl stretching	dp
1390(w)	1384(s)	1387(m)	1389(m)	N-phenyl stretching	p
1582(vs)	1581(w)	1583(w)	1588(w)	ring C—C stretching	dp
1617(w)	1615(s)	1615(vs)	1617(s)	ring C—C stretching	p

[a] Note: p, polarized; dp, depolarized; w, weak; m, middle; s, strong and vs, very strong. [b] Reference 31. [c] Reference 32.

TABLE 1. Parameters for the Calculation of EF[a]

						relative intensity (I)	
spectra	N_A	M (mol/L)	$V_{solution}$	S_{sub}	S_{laser}	1648 cm^{-1}	1364 cm^{-1}
SERRS	constant	10^{-11}	2 μL	0.50 cm^2	2 μm in diameter	20350 ± 680	15500 ± 700
RRS		10^{-2}				291200 ± 6200	258600 ± 6600

[a] Note: The two corresponding peaks marked with crosses in Figure 6 are used for the calculation of EF, and the intensities are fitted with Gaussian curves.

effect in the ultrahigh SERS enhancements of the wrinkled NPG films.

Although NPG itself is a good SERS substrate and significant enhancements can be achieved from the nanosized gold ligaments and nanopores, there is inadequate electromagnetic coupling between the gold ligaments because of the large interligament distance and the in-plane feature of the main nanostructure. For the electromagnetic enhancement of SERS, electromagnetic "hot-spots" at nanogaps and sharp nanotips have been demonstrated to play a crucial role in the overall SERS enhancements.[5] The wrinkling treatment can result in stronger electromagnetic coupling between the vertically standing nanoporous films that are parallel to the incident lasers. The ductile cracking of the 26 nm NPG films, different from the brittle failure of the 12 nm NPG, produces a large number of microcracks with various gap widths, which can generate plenty of "hot spots" by the local optical coupling with suitable gap width (Figure 3b). Moreover, the sharp nanotips of the broken ligaments (Figure 3d,e) can also provide strongly localized electromagnetic fields for ultrahigh SERS enhancements[34] because of the additional lightning rod effect.[35]

CONCLUSION

We have developed a novel wrinkled substrate with abundant "hot spots" for ultrahigh SERS enhancements by thermal contraction of prestrained PS veneered by 100 nm NPG films. The winkling treatment turns the planar NPG films to a vertical 3D nanostructure with plentiful nanogaps and sharp nanotips that act as electromagnetic "hot-spots" when interacting with incident light. The SERS enhancement of the wrinkled NPG is over 100 times higher than that of the as-prepared NPG, which yields a local enhancement factor of $\sim 10^9$.

EXPERIMENTAL METHODS

Sample Preparation. Three 100 nm thick NPG films with pore sizes of 12, 26, and 38 nm were prepared by selective dissolution of silver from $Au_{35}Ag_{65}$ (atom %) alloy leaves using 71% nitric acid at room temperature for 10, 60, and 360 min, respectively.[21−24] After being carefully washed with distilled water (18.2 MΩ cm), the as-prepared NPG films with an area of 2 cm × 2 cm were physically attached to the prestrained PS and heated at 80 °C for 1 h to strengthen the bonding between NPG and PS. At this temperature, both the prestrained PS and the NPG films are very stable, and detectable volume contraction of PS and nanopore coarsening cannot be found. Finally, the NPG/PS composites (as shown in Figure 1) were heated at 160 °C for 6 min.

Materials and Equipments. The prestrained PS (KSF50-C, Grafix) is an amorphous polymer which will shrink when heating up to a temperature above its glass transition point. The glass transition temperature of the PS that was used in the experiment is ~95 °C, and the melting temperature is ~240 °C. The temperature that we used for the heating treatment is 160 °C for 6 min, which is higher than the glass transition temperature but lower than the melting temperature, leading to more than half volume shrinking of the PS. Crystal violet (CV, Aldrich) and Rhodamine 6G (R6G, Aldrich) in methanol solutions were used as probe molecules for SERS measurements. Human serum albumin (HSA, Aldrich) was used as a spacer layer for fluorescence imaging.[36] The structure features of as-prepared and wrinkled NPG films were investigated by scanning electron microscope (SEM, JIB-4600F) and scanning transmitting electron microscope (STEM, JEM-2100F). Fluorescence images were taken with Olympus BX51 microscope (20× dry objective and mercury burner USH-1030 L lamp). A micro-Raman spectrometer (Renishaw InVia RM 1000) with incident wavelength of 514.5 nm and 632.8 nm was used in the Raman study. The laser powers were set at very low values (0.06mW for R6G detection and 0.3mW for CV detection) to avoid possible damage by the laser irritation. The accumulation time of each spectrum is 50 s.

Fluorescence Measurements. The wrinkled NPG substrates were immersed in a 20 μM HSA solution for more than 24 h, and then taken out and washed with distill water before they dried in the air. A 2 μL droplet of 10^{-10} M CV methanol solution was dropped on the HSA-modified substrates. After drying, the fluorescence images were taken from the centers of the droplets.

Acknowledgment. This work was sponsored by "Global COE for Materials Research and Education" and "World Premier International Research Center (WPI) Initiative" by the MEXT, Japan, and was also supported by "Iketani Science and Technology Foundation", "Murata Science Foundation", and "Inamori Foundation".

Supporting Information Available: Detailed description on the contraction rate effect in the SERS activity and the enhancement variation of different Raman modes of CV molecules. This material is available free of charge *via* the Internet at http://pubs.acs.org.

REFERENCES AND NOTES

1. Moskovits, M. Surface-Enhanced Spectroscopy. *Rev. Mod. Phys.* **1985**, *57*, 783–826.
2. Nie, S.; Emory, S. R. Probing Single Molecules and Single Nanoparticles by Surface-Enhanced Raman Scattering. *Science* **1997**, *275*, 1102–1106.
3. Li, J. F.; Huang, Y. F.; Ding, Y.; Yang, Z. L.; Li, S. B.; Zhou, X. S.; Fan, F. R.; Zhang, W.; Zhou, Z. Y.; Wu, D. Y.; *et al.* Q. Shell-Isolated Nanoparticle-Enhanced Raman Spectroscopy. *Nature* **2010**, *464*, 392–395.
4. Yao, J.; Le, A.-P.; Gray, S. K.; Moore, J. S.; Roger, J. A.; Nuzzo, R. G. Functional Nanostructured Plasmonic Materials. *Adv. Mater.* **2010**, *22*, 1102–1110.
5. Fang, Y.; Seong, N.-H.; Dlott, D. D. Measurement of the Distribution of Site Enhancement in Surface-Enhanced Raman Scattering. *Science* **2008**, *321*, 388–391.
6. Sau, T. K.; Rogach, A. L.; Jäckel, F.; Klar, T. A.; Feldmann, J. Properties and Applications of Colloidal Nanospherical Nobel Metal Nanoparticles. *Adv. Mater.* **2009**, *21*, 1–21.
7. Lierman, V.; Yilmaz, C.; Bloomstein, T. M.; Somu, S.; Echegoyen, Y.; Busnaina, A.; Cann, S. G.; Krohn, K. E.; Marchant, M. F.; Rothschild; *et al.* Convective Directed Assembly Process for the Fabrication of Periodic Surface Enhanced Raman Spectroscopy Substrates. *Adv. Mater.* **2010**, *22*, 4298–4302.
8. Polman, A. Plasmonic Applied. *Science* **2008**, *322*, 868–869.
9. Banholzer, M. J.; Millstone, J. E.; Qin, L.; Mirkin, C. A. Rationally Designed Nanostructures for Surface-Enhanced Raman Spectroscopy. *Chem. Soc. Rev.* **2008**, *37*, 885–897.
10. Schuck, P. J.; Fromm, D. P.; Sundaramurthy, A.; Kino, G. S.; Moerner, W. E. Improving the Mismatch between Light and Nanoscale Objects with Gold Bowtie Nanoantennas. *Phys. Rev. Lett.* **2005**, *94*, 017402–1.
11. Lim, D.-K.; Jeon, K.-S.; Kim, M. H.; Nam, J.-M.; Suh, Y. D. Nanogap-Engineerable Raman-Active Nanodumbbells for Single-Molecule Detection. *Nat. Mater.* **2010**, *9*, 60–67.

12. Kneipp, K.; Wang, Y.; Kneipp, H.; Perelman, L. T.; Itzkan, I.; Dasari, R. R.; Feld, M. S. Single Molecule Detection Using Surface-Enhanced Raman Scattering (SERS). *Phys. Rev. Lett.* **1997**, *78*, 1667–1670.
13. Sharaabi, Y.; Shegai, T.; Haran, G. Two-State Analysis of Single-Molecule Raman Spectra of Crystal Violet. *Chem. Phys.* **2005**, *318*, 44–49.
14. Le Ru, C. E.; Meyer, M.; Etchegoin, P. G. Proof of Single-Molecule Sensitivity in Surface Enhanced Raman Scattering (SERS) by Means of a Two-Analyte Technique. *J. Phys. Chem. B* **2006**, *110*, 1944–1948.
15. Wei, H.; Håkanson, U.; Yang, Z.; Höök, F.; Xu, H. Individual Nanometer Hole-Particle Pairs for Surface-Enhannced Raman Scattering. *Small* **2008**, *4*, 1296–1300.
16. Bowden, N.; Brittain, S.; Evans, A. G.; Hutchison, J. W.; Waitesides, G. M. Spontaneous Formation of Ordered Structures in Thin Films of Metals Supported on an Elastomeric Polymer. *Nature* **1998**, *393*, 146–149.
17. Lacour, S. P.; Wagner, S.; Huang, Z.; Suo, Z. Stretchable Gold Conductors on Elastomeric Substrates. *Appl. Phys. Lett.* **2003**, *82*, 2404.
18. Fu, C. C.; Ossato, G.; Long, M.; Digman, M. A.; Gopinathan, A.; Lee, L. P.; Gratton, E.; Khine, M. Bimetallic Nanopetals for Thousand-Fold Fluorescence Enhancements. *Appl. Phys. Lett.* **2010**, *97*, 203101.
19. Fu, C. C.; Grimes, A.; Long, M.; Ferri, C. G. L.; Rich, B. D.; Ghosh, S.; Lee, L. P.; Gopinathan, A.; Khine, M. Tunable Nanowrinkles on Shape Memory Polymer Sheets. *Adv. Mater.* **2009**, *21*, 4472–4476.
20. Yang, S.; Khare, K.; Kin, P.-C. Harnessing Surface Wrinkle Patterns in Soft Matter. *Adv. Funct. Mater.* **2010**, *20*, 2550–2564.
21. Qian, L. H.; Yan, X. Q.; Fujita, T.; Inoue, A.; Chen, M. W. Surface-Enhanced Raman Scattering of Nanoporous Gold: Smaller Pore Sizes Stronger Enhancements. *Appl. Phys. Lett.* **2007**, *91*, 083105.
22. Erlebacher, J.; Seshadri, R. Hard Materials with Tunable Porosity. *MRS Bull.* **2009**, *34*, 561–566.
23. Ding, Y.; Kim, J. Y.; Erlebacher, J. Nanoporous Gold Leaf: "Ancient Technology"/Advanced Material. *Adv. Mater.* **2004**, *16*, 1897–1900.
24. Erlebacher, J.; Aziz, J. M.; Karma, A.; Dimitrov, N.; Sieradzki, K. Evolution of Nanoporosity in Dealloying. *Nature* **2001**, *410*, 450–453.
25. Fujita, T.; Qian, L. H.; Inoke, K.; Erlebacher, J.; Chen, M. W. Three-Dimensional Morphology of Nanoporous Gold. *Appl. Phys. Lett.* **2008**, *92*, 251902.
26. Li, R.; Sieradzki, K. Ductile-Brittle Transition in Random Porous Au. *Phys. Rev. Lett.* **1992**, *68*, 1168–1171.
27. Kudelski, A. Raman Studies of Rhodamine 6G and Crystal Violet Sub-Monolayers on Electrochemically Roughened Silver Substrates: Do Dye Molecules Adsorb Preferentially on Highly SERS-Active Sites?. *Chem. Phys. Lett.* **2005**, *414*, 271–275.
28. Cai, W. B.; Ren, B.; Li, X. Q.; She, C. X.; Liu, F. M.; Cai, X. W.; Tian., Z. Q. Investigation of Surface-Enhanced Raman Scattering from Platinum Electrodes Using a Confocal Raman Microscope: Dependence of Surface Roughening Pretreatment. *Surf. Sci.* **1998**, *406*, 9–22.
29. McFarland, A. D.; Young, M. A.; Dieringer, J. A.; Van Duyne, R. P. Wavelength-Scanned Surface-Enhanced Raman Excitation Spectroscopy. *J. Phys. Chem. B* **2005**, *109*, 11279–11285.
30. Le Ru, E. C.; Blackie, E.; Meyer, M.; Etchegoin, P. G. Surface-Enhanced Raman Scattering Enhancement Factors; A Comprehensive Study. *J. Phys. Chem. C* **2007**, *111*, 13794–13803.
31. Sackmann, M.; Bom., S.; Balster, T.; Materny, A. Nanostructured Gold Surfaces as Reproducible Substrates for Surface-Enhanced Raman Spectroscopy. *J. Raman Spectrosc.* **2007**, *38*, 277–282.
32. Cañamares, M. V.; Chenal, C.; Birke, R. L.; Lombardi, J. R. DFT, SERS, and Single-Molecule SERS of Crystal Violet. *J. Phys. Chem. C* **2008**, *112*, 20295–20300.
33. Angeloni, L.; Smulevich, G.; Marzocchi, M. P. Resonance Raman Spectrum of Crystal Violet. *J. Raman Spectrosc.* **1979**, *8*, 305–308.
34. Qian, L. H.; Inoue, A.; Chen, M. W. Large Surface Enhanced Raman Scattering Enhancements from Fracture Surfaces of Nanoporous Gold. *Appl. Phys. Lett.* **2008**, *92*, 093113.
35. Liao, F. P.; Wokaun, A. Lightning Rod Effect in Surface Enhanced Raman Scattering. *J. Chem. Phys.* **1982**, *76*, 751–752.
36. Lang, X. Y.; Guan, P. F.; Zhang, L.; Fujita, T.; Chen, M. W. Size Dependence of Molecular Fluorescence Enhancement on Nanoporous Gold. *Appl. Phys. Lett.* **2010**, *96*, 073701.